

The Generalized Droop Formula

Alberto Bononi, *Senior Member, IEEE*, Jean-Christophe Antona, Matteo Lonardi, *Student Member, IEEE*, Alexis Carbo-Méseguer and Paolo Serena, *Member, IEEE*

Abstract—We present a theoretical model that fully supports the recently disclosed generalized droop formula (GDF) for calculating the signal-to-noise ratio (SNR) of constant-output power (COP) amplified dispersion-uncompensated coherent links operated at very low SNR. We compare the GDF to the better known Gaussian noise (GN) model. A key finding is that the end-to-end model underlying the GDF is a concatenation of per-span first-order regular perturbation (RP1) models with end-span power renormalization. This fact allows the GDF to well reproduce the SNR of highly nonlinear systems, well beyond the RP1 limit underlying the GN model. The GDF is successfully extended to the case where the bandwidth/modes of the COP amplifiers are not entirely filled by the transmitted multiplex. Finally, the GDF is extended to constant-gain (CG) amplifier chains and is shown to improve on known GN models of highly nonlinear propagation with CG amplifiers.

Index Terms—Optical amplifiers, Signal Droop, Split-step Fourier method, GN model.

I. INTRODUCTION

Amplified spontaneous emission (ASE)-induced signal droop in constant output power (COP) amplifier chains was studied long ago [1]. Today's submarine systems basically all use COP amplifiers, but most analytical models for single-mode transmission do assume constant-gain (CG) amplifiers, with a few exceptions (e.g., [2]). In the context of space-division multiplexed (SDM) submarine transmissions, the term "droop" was introduced a few years ago by Sinkin *et al.* [3], [4], who revived the droop problem in COP amplified SDM links. Antona *et al.* [5], [6] recently proposed a new expression of the received

signal to noise ratio (SNR) in very-long haul, low-SNR dispersion-uncompensated submarine links with coherent detection, which we here call the generalized droop formula (GDF), and showed that for single-mode COP-amplified links the GDF is more precise than the SNR predicted by the widely-used Gaussian Noise (GN) model [7]–[10], which assumes CG amplifiers. The GDF accounts for both signal and ASE droop, both in the linear and in the nonlinear regime. Extensions of the GDF to account for other sources of power rearrangement in the transmission fiber were also proposed [5], [6].

This paper, which is an extension of [11], aims to recast the heuristic derivations in [5], [6] on solid theoretical footings, and to extend the comparisons of the GDF against the GN model and its extension to COP amplifiers [2]. One of the key theoretical findings of this paper is that the end-to-end model underlying the GDF is a concatenation of per-span first-order regular perturbation (RP1) models [12] with end-span power renormalization. This fact allows the GDF to well reproduce the SNR of highly nonlinear systems, well beyond the RP1 limit underlying the GN model [13]–[15]. This multi-stage RP1 is reminiscent of multi-stage backpropagation [16], [17] that combines the benefits of split-step and perturbation-based approaches.

The GDF theory is then extended to the more general case where significant out-of-band ASE is present in the system, yielding a new SNR expression that we call the COP-GDF. While working out the extended theory, we find deep connections also with constant-gain (CG) amplifier chains with significant nonlinear signal-ASE interactions, for which extensions of the GN theory are known [18], [19]. We here propose a new formula, which we call the CG-GDF. All formulas are checked against accurate split-step Fourier method (SSFM) simulations. In particular, COP-GDF and CG-GDF always show the best match with simulations among all known formulas.

The paper is organized as follows. Sections II and III introduce the system model and derive the additive and rearrangement droops. Sec. IV derives the basic GDF, discusses its implications and introduces upper and lower bounds to the GDF. Sec. V presents numerical comparisons of theory against simulations, and GDF against both its approximations and against the GN

Manuscript received xxxxxxxx xx, xxxx; accepted xxxxxxxx xx, xxxx. Date of publication xxxxxxxx xx, xxxx; date of current version xxxxxxxx xx, xxxx.

A. Bononi, P. Serena, M. Lonardi are with the Dipartimento di Ingegneria e Architettura, Università di Parma, Parma 43124, Italy (corresponding author e-mail: alberto.bononi@unipr.it). J.-C. Antona and A. Carbo-Méseguer are with Alcatel Submarine Networks, Villarsaux, France.

Color versions of one or more of the figures in this paper are available online at <http://ieeexplore.ieee.org>.

Digital Object Identifier xx.xxxx/JLT.xxxx.xxxxxx.

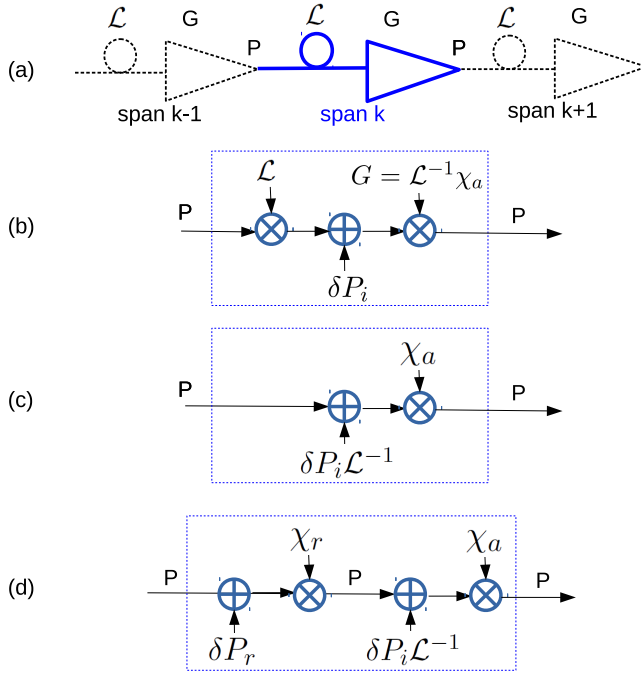


Figure 1. (a) Chain of spans with loss \mathcal{L} with amplifiers with constant output power P and ASE equivalent input power δP_i . Gain must be $G = \mathcal{L}^{-1}\chi_a$ (see text), with $\chi_a < 1$ the ASE-induced power droop. (b) Span power block diagram. (c) Equivalent diagram with loss factored out. (d) Added block diagram also of fiber span with redistribution power δP_r and renormalization to P by a redistribution power droop $\chi_r < 1$.

formula. Sec. VI extends the GDF to the case when ASE has a larger spectral occupancy than the useful signal. Sec. VII discusses the CG case and derives the new CG-GDF expression. Sec. VIII concludes the paper.

II. DROOP INDUCED BY POWER ADDITION

Consider the transmission of a mode/wavelength division multiplexed (M/WDM) signal, composed of M spatial modes (each corresponding to two orthogonal polarizations) each composed of an N_c -channel Nyquist-WDM system [20] over a total bandwidth B , along a chain of N identical multi-mode/core fiber (MF) spans. All spans have loss $\mathcal{L} < 1$ and are followed by an end-span amplifier having a total constant output power (COP) equal to P . We assume the multiplex total launched power is P , and that loss \mathcal{L} and amplifier gain G are the same at all wavelengths and modes. We also assume the amplifier has a filter that suppresses all out-of band/mode ASE noise, so that ASE and signal spectra are flat over the same bandwidth B . The Nyquist-WDM assumption and the assumption that ASE and signal exist on the same spectral range will be relaxed in Section VI.

As seen in Fig. 1(a), the chain has at each span k a total input power P , and a total output power P .

Hence in the ideal case of noiseless amplifiers, the amplifier gain $G = \mathcal{L}^{-1}$ exactly compensates the loss. The span block diagram for real amplifiers is shown in Fig. 1(b), where an equivalent input ASE noise power $\delta P_i = Mh\nu FB$ (where h is Planck's constant, ν is the multiplex center frequency, F is the noise figure [21], B the amplification bandwidth and M is the number of modes) is injected in the amplifier, hence the gain $G = \mathcal{L}^{-1}\chi_a$ must decrease by a *droop* factor $\chi_a < 1$ from the ideal case to “squeeze” the transiting signal and make room for the local ASE noise in the output power budget P . By shifting back the term \mathcal{L}^{-1} upstream of the addition block (i.e., by “factoring out” the loss) the block of Fig. 1(b) is seen to be equivalent to that in Fig. 1(c), from which we read the span input-output power budget as: $(P + \delta P_i \mathcal{L}^{-1})\chi_a = P$, and thus deduce the droop

$$\chi_a = (1 + \frac{\delta P_i \mathcal{L}^{-1}}{P})^{-1} \triangleq (1 + SNR_{a1}^{-1})^{-1} \quad (1)$$

where $\delta P_i \mathcal{L}^{-1}$ is the output ASE that would be generated by an end-span amplifier with gain \mathcal{L}^{-1} , and we implicitly defined SNR degraded at the single amplifier as

$$SNR_{a1} \triangleq \frac{P}{\delta P_i \mathcal{L}^{-1}}. \quad (2)$$

The droop is in fact the total power gain (in fact, a loss) of each amplified span, so that the desired multiplex signal power at the output of the N -th amplifier is

$$P_s(N) = P \prod_{k=1}^N \mathcal{L}G = P\chi_a^N \quad (3)$$

which tells us that the desired signal becomes weaker along the nominally transparent line because of the accumulation of ASE which reduces the amplifier gain G because of the COP constraint. The accumulated ASE at the output of the N -span chain (over all modes and amplified WDM bandwidth B) is thus

$$P_a(N) = P - P_s(N) = P(1 - \chi_a^N). \quad (4)$$

By equating (3),(4) we find that signal and ASE powers become equal at $N \cong \ln 2 \cdot SNR_{a1}$.

Note that the above analysis remains unchanged if the amplifiers were noiseless, but an external lumped crosstalk (e.g., power leaking from a competing optical multiplex of power P crossing an optical multiplexer/demultiplexer together with our multiplex of interest at an optical node before the final optical amplification, or, e.g., transmitter impairments at the booster amplifier) of power $\delta P_i = \alpha_{ex}P$ were injected in its place, where α_{ex} is the external crosstalk coefficient. In presence of both ASE and external crosstalk the droop χ_a in (1), that we more generally call the *addition*

droop, uses an added power $\delta P_i = Mh\nu FB + \alpha_{ex}P$, where uncorrelation between the two noise sources is assumed when summing power.

III. DROOP INDUCED BY POWER REDISTRIBUTION

The transmission fiber is indeed not ideal and operates a power redistribution during propagation because of several physical mechanisms. Let's for the moment concentrate on one of these, namely, the nonlinear Kerr effect. Focus on Fig. 1(c) where the fiber loss has been factored out. We now apply a first-order regular perturbation approximation of the Kerr distortion generated within span k , called nonlinear interference (NLI), as in the GN and similar perturbative models [7], [8], [10]. We then impose that the power in/out of the fiber be conserved. Thus, we get a power-flow diagram of the fiber+amplifier block as depicted in Fig. 1(d), where now the power redistribution during propagation appears as a new input sub-block in which a perturbation $\delta P_r = \alpha_{NL}P^3$ is added to the input signal P (α_{NL} is the per-span NLI coefficient [22]), and then a *redistribution droop* χ_r forces the perturbed signal back to power P , namely, $(P + \delta P_r)\chi_r = P$. This yields

$$\chi_r = (1 + \frac{\delta P_r}{P})^{-1} \triangleq (1 + SNR_{r1}^{-1})^{-1} \quad (5)$$

where we implicitly defined the SNR degraded at the single amplifier by the redistribution mechanism as

$$SNR_{r1} \triangleq \frac{P}{\delta P_r} = \frac{1}{\alpha_{NL}P^2} \quad (6)$$

where the second equality holds specifically for the NLI redistribution mechanism.

In other terms, we first apply a per-span RP1 perturbation, and then re-normalize signal plus perturbation power at fiber end, thus reducing at each span the power-divergence problem intrinsic in the RP1 approximation [12]. Other redistribution mechanisms for which the above theory applies verbatim are:

1) the thermally-induced guided-acoustic wave Brillouin scattering (GAWBS) [23], for which $\delta P_r = \gamma_{GAWBS}\ell P$, where γ_{GAWBS} [km^{-1}] is the GAWBS coefficient, and ℓ [km] is the span length;

2) the inter-mode/core linear crosstalk in the MF, for which $\delta P_r = \gamma_X\ell P$, where γ_X [km^{-1}] is the crosstalk coefficient [24].

Thus including all three (uncorrelated) effects, we have in (5),(6): $\delta P_r = \alpha_{NL}P^3 + (\gamma_{GAWBS} + \gamma_X)\ell P$.

IV. SIGNAL TO NOISE RATIO

According to the proposed per-span power-flow diagram in Fig. 1(d), the total span power gain seen by the transiting signal, i.e., the overall span droop, is

the product of addition and redistribution droops: $\chi \triangleq \chi_r\chi_a$. By the same reasoning as in (3),(4), if the launch power is P , then the desired multiplex signal power at the output of the N -th amplifier is $P_s(N) = P\chi^N$ and therefore by the constant output power constraint the accumulated *addition+redistribution noise* at the output of the N -span chain (over all modes and amplified WDM bandwidth B) is $P_a(N) + P_r(N) = P(1 - \chi^N)$.

Hence the optical SNR (OSNR) at the output of the chain from amplifiers 1 to N , i.e., the ratio of total multiplex signal power to total noise power at the output of the N -th amplifier, using (1),(5) is obtained as,

$$OSNR = \frac{1}{[(1 + SNR_{a1}^{-1})(1 + SNR_{r1}^{-1})]^N - 1} \quad (7)$$

which is the generalized droop formula (GDF) derived for the first time in [5], [6] based on heuristic arguments. The above derivation puts the GDF on a solid theoretical footing. Please note a key assumption of the GDF model: the power additions expressed by the power block diagram, Fig. 1, tacitly imply that the noise sources injected at each span are uncorrelated from all others, and thus, in particular, assuming an incoherent accumulation of NLI.

The GDF can be re-arranged into the key formula [5], [6]

$$1 + \frac{1}{OSNR} = \left[\left(1 + \frac{1}{SNR_{a1}} \right) \left(1 + \frac{1}{SNR_{r1}} \right) \right]^N \quad (8)$$

which we call the *product rule for inverse droop*. It hints at the generalization [5], [6]

$$1 + \frac{1}{OSNR} = \prod_{k=1}^N \left(1 + \frac{1}{SNR_{a1k}} \right) \left(1 + \frac{1}{SNR_{r1k}} \right) \quad (9)$$

for an inhomogeneous chain, where SNR_{a1k} is the local ASE-reduced OSNR at amplifier k , and similarly SNR_{r1k} for redistribution noise. We prove this generalization in Appendix A.

We conclude this section with a key observation. When the dominant part of the power spectral density (PSD) of each of the above impairments remains flat as the input signal PSD, then the per-tributary signal to noise ratio SNR for this flat-loss, flat-gain system will remain equal to $OSNR$, since both signal and noises get filtered over the same tributary bandwidth and mode. Hence from now on, we will drop the “O” in the OSNR, and treat P and B as the launched input power and bandwidth of each tributary. In section VI we will generalize the per-tributary SNR expression to the case where ASE occupies a larger bandwidth/number of modes than the signal multiplex.

SNR approximations

We derive here upper and lower bounds to the GDF. Define

$$SNR_1 \triangleq (SNR_{a1}^{-1} + SNR_{r1}^{-1})^{-1} \quad (10)$$

as the SNR degraded by the total noise generated at a single span. Let $x \triangleq SNR_1^{-1}$, which is normally a very small term. Then, as proposed in [5], the GDF denominator can be bounded as: $\chi^{-N} - 1 \geq (1+x)^N - 1 \geq Nx(1 + \frac{1}{2}(N-1)x)$ by expanding to 2nd order in Taylor. Thus an upper-bound to the GDF is

$$SNR \leq \frac{SNR_s}{1 + \frac{1}{2}(1 - \frac{1}{N})(SNR_s)^{-1}} \quad (11)$$

where

$$SNR_s \triangleq \frac{1}{Nx} \equiv \frac{SNR_1}{N} \quad (12)$$

is the SNR we would calculate with the standard noise accumulation formula for constant-gain amplifiers. We call it the *standard SNR*.

Now let $y = \frac{1}{2}(1 - \frac{1}{N})Nx \geq 0$. Since $(1+y)^{-1} \geq 1-y$, then we can lower-bound the upper-bound (11) and luckily get a lower bound to the GDF-SNR as well:

$$SNR \geq \frac{1 - \frac{1}{2}(1 - \frac{1}{N})Nx}{Nx} = SNR_s - \frac{1}{2}(1 - \frac{1}{N}). \quad (13)$$

To understand the scope of the above approximations, Fig. 2(a) shows in black solid line a plot of the GDF-SNR¹:

$$SNR \cong ((1 + SNR_1^{-1})^N - 1)^{-1} \quad (14)$$

versus the standard $SNR_s \equiv SNR_1/N$. The figure also shows its upper-bound (UB) eq. (11) and lower-bound (LB) eq. (13) (both dash-dotted), and the SNR_s itself (dotted). Fig. 2(b) shows the same as (a), but with SNRs expressed in dB. The curves in Fig. 2 were obtained for $N = 100$, but they remain essentially unchanged for any $N \geq 40$.

We observe in Fig. 2(a) and can prove analytically that: i) the LB (13) crosses zero at $SNR_s = \frac{N-1}{2N}$ and becomes negative (not physically acceptable) below that; ii) the gap from SNR_s to GDF (and to all its approximations) converges for increasing SNR_s to the asymptotic value $\frac{1}{2}(1 - \frac{1}{N})$, and the gap from SNR_s to GDF exceeds 90% of its asymptotic value at $SNR_s > 1.66$ (2.2dB) for any N . The constant gap in linear units translates into a variable gap when SNRs are in dB, i.e., to a small dB-gap at large SNR_s and a large dB-gap at lower SNR_s . The dB plot also does not clearly show the $\sim 1/2$ asymptotic linear gap.

¹Since SNR_{a1}^{-1} and SNR_{r1}^{-1} are normally very small, then the product $SNR_{a1}^{-1}SNR_{r1}^{-1}$ is a higher-order negligible term. Hence the GDF (7) and expression (14) are practically identical.

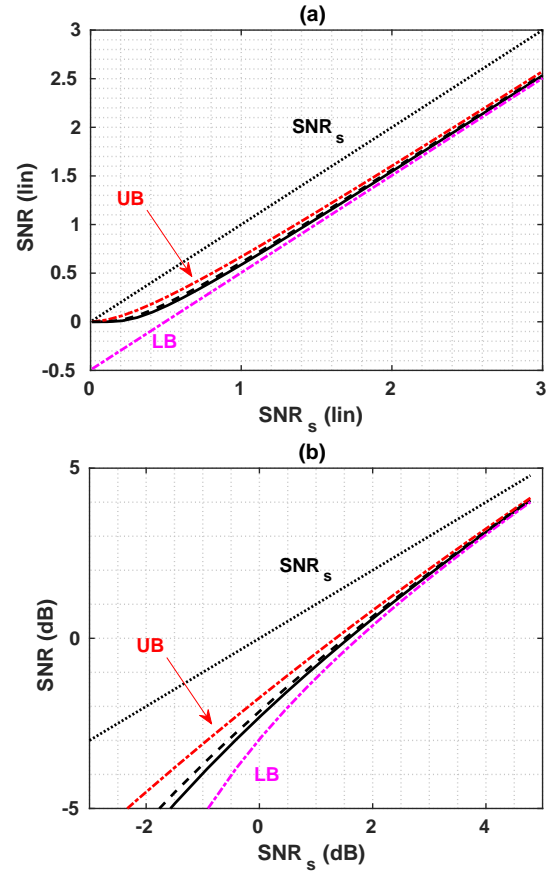


Figure 2. (a) Solid: GDF (14) versus the standard SNR: $SNR_s = SNR_1/N$. Dash-dot: Upper-bound (UB) eq. (11) and Lower-Bound (LB) eq. (13). Dotted: SNR_s . Dashed: approximation (15). (b) Corresponding figure when SNRs are in dB. Curves obtained for $N = 100$, but they remain essentially unchanged for any $N \geq 40$.

These observations will be useful when interpreting the numerical SNR results in Section V.

Our best approximation to the GDF (which also turns out to be a tighter upper-bound) is shown in dashed line in Fig. 2, and can be obtained by taking $10 \log_{10}(\cdot)$ of each side of eq. (11) and then linearizing the logarithm. The resulting expression in dB is:

$$SNR(dB) \geq SNR_s(dB) - \frac{e^{dB} \cdot \frac{1}{2}(1 - \frac{1}{N})}{SNR_s} \quad (15)$$

where SNR_s without (dB) indicates its linear value, $e^{dB} \triangleq 10 \log_{10}(e) \cong 4.34$, and e is Neper's number.

To make the physical meaning of the above approximations to the GDF explicit, let's focus on the case of single-mode fibers ($M = 1$), with ASE and NLI only. Define

$$\beta \triangleq h\nu FBL^{-1} \quad (16)$$

as the ASE power (per mode) generated at the output of each amplifier of gain \mathcal{L}^{-1} over the per-tributary receiver bandwidth B . Then from (10),(2),(6) we get

$$SNR_s \equiv \frac{1}{N(\frac{\beta}{P} + \alpha_{NL}P^2)} \quad (17)$$

where in (2) we used $\delta P_i \mathcal{L}^{-1} = \beta$, and the α_{NL} term is nominally the single-span coefficient computed over the same per-tributary bandwidth B as β (more on α_{NL} in Appendix B). We recognize the standard SNR (17) to be the SNR of the well-known (incoherent) GN formula [10]. The obtained upper and lower bounds are therefore approximations of the GDF formula based solely on the value of the GN-SNR.

Although the above GN and GDF models assume uncorrelated NLI span by span, in numerical computations we can approximately account for the NLI span-by-span correlation by first calculating the NLI coefficient of the entire link (using either the extended GN (EGN) model [25]–[28] for the selected modulation format or by using SSFM simulations as described in Appendix B) and then dividing by N , so that now the α_{NL} to be used in the (coherent) GN² and GDF is a span-averaged coefficient and in general depends on N .

V. NUMERICAL CHECKS

We present here three single-mode case studies with quasi Nyquist-WDM signals where we verify the above formulas against SSFM simulations:

case A is the 228x78km polarization-division multiplexed (PDM) quadrature phase-shift keying (QPSK) WDM uncompensated link analyzed in [5]. The propagation fiber was an EX2000TM (loss 0.169 dB/km, fiber nonlinear coefficient $n_2 = 2.5 \cdot 10^{-20}$ m²/W, effective area 110 μm^2 , dispersion 20.7 ps/nm/km). Optical amplifiers had a noise figure F of 8dB. The number of channels was 16, with channel spacing 37.5 GHz and symbol rate 34.17 Gbaud. SSFM simulations were carried out with a simulated bandwidth 60 times the symbol rate, and ASE was removed outside the WDM bandwidth. The number of transmitted symbols was 64800.

case B is the 190x78km PDM 16-quadrature amplitude modulation (16QAM) link analyzed in [5]. All data are the same as in case A, except for the number of spans (now 190) and the modulation format. The number of transmitted symbols was 2^{16} .

case C is the 40x120km PDM-QPSK link analyzed in [2, Fig. 3]. The propagation fiber was a non-zero dispersion shifted fiber (NZDSF) (loss 0.22 dB/km, fiber NL coefficient $n_2 = 2.6 \cdot 10^{-20}$ m²/W, effective area 70.26 μm^2 , dispersion 3.8 ps/nm/km). Noise figure F was 5dB. The number of channels was 15, with channel spacing 50 GHz and symbol rate 49 Gbaud. Again the simulated bandwidth was 60 times the symbol rate, and

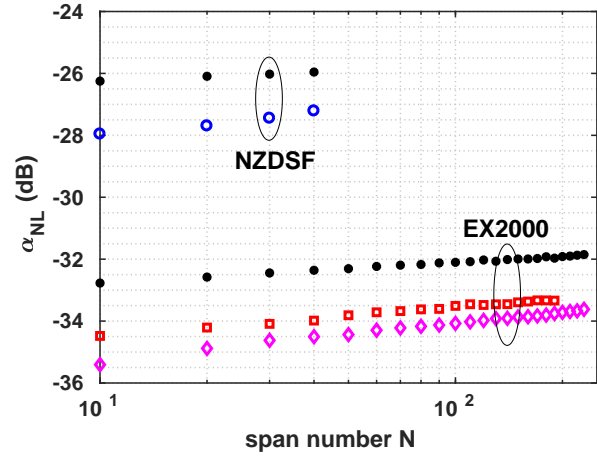


Figure 3. Values in dB of span-averaged NLI coefficient α_{NL} (mW⁻²) versus spans N , used in theoretical formulas for the 3 case studies (diamonds case A, squares case B, circles case C). Also, filled circles show values for Gaussian modulation.

ASE was removed outside the WDM bandwidth. The number of transmitted symbols was 2^{13} .

We accounted just for ASE and NLI, and the GDF formula explicitly is

$$SNR = \frac{1}{\left[\left(1 + \frac{\beta}{P} \right) (1 + \alpha_{NL} P^2) \right]^N - 1}. \quad (18)$$

For all 3 cases, we will present results at the stated number of spans, as well as some results at lower span numbers, all multiples of 10. Fig. 3 shows the values of the span-averaged α_{NL} we have used in the theoretical formulas in the 3 cases (diamonds for case A, squares for case B, circles for case C), along with the values for Gaussian modulation (filled circles). We note in passing that an α_{NL} that grows with N is an indication of self-nonlinearity becoming more important than cross-nonlinearity as N increases, which is typical of small WDM systems [22].

We begin by presenting in Fig. 4 the received SNR versus transmitted power per channel P for all 3 cases at their maximum distance. In all 3 sub-figures we report: the GN formula (17) (dashed black) and the GDF (18) (solid blue), along with their linear and nonlinear asymptotes (dotted); the SSFM simulations at constant output power (symbols: diamonds for case A, squares for case B, circles for case C); the upper and lower bounds UB (11), LB (13) (both dash-dotted), and the approximation (15) (dashed). Values of α_{NL} estimated from low-power simulations and used in theoretical formulas were: $\alpha_{NL} = [4.34, 4.63, 19.01] \times 10^{-4}$ (mW⁻²) for cases A,B,C, respectively. These can be read from Fig. 3.

We first note in all cases the very good fit of the GDF with SSFM simulations, not only in cases A and

²We should more correctly use the acronym EGN everywhere, since α_{NL} always accounts for the modulation format. We opted, however, to keep GN since the term is more widespread.

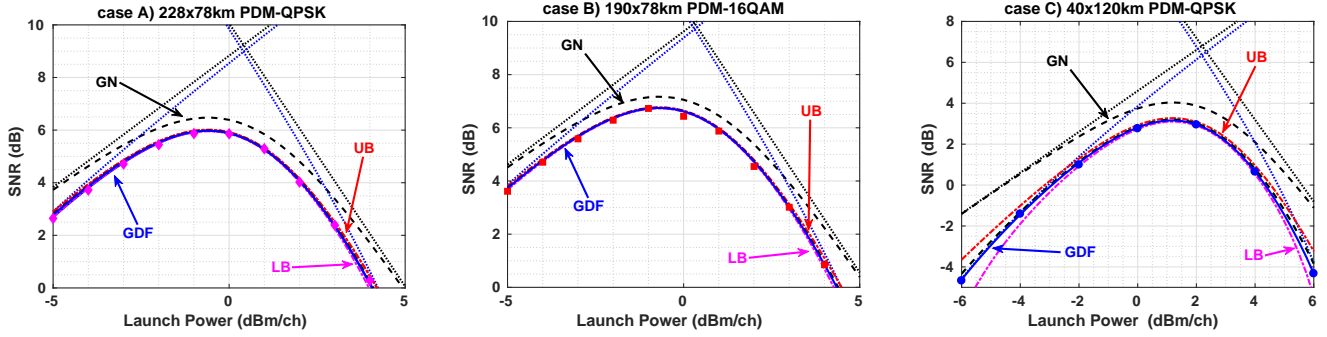


Figure 4. SNR(dB) versus power per channel P (dBm) for: **case A)** 228x78km EX2000 uncompensated link, 34.17 Gbd PDM-QPSK, 16-channel @ 37.5GHz spacing [5]; **case B)** 190x78km EX2000 uncompensated link, 34.17 Gbd PDM-16QAM, 16-channel @ 37.5GHz [5]; **case C)** 40x120km NZDSF uncompensated link, 49-Gbd PDM-QPSK, 15-channel @ 50GHz [2]. In each plot: Symbols: SSFM simulations. Blue solid: GDF eq. (18). Black dashed: GN formula eq. (17). Linear and nonlinear asymptotes also shown in dotted lines. GDF Approximations: Red dash-dotted: upper-bound (UB) (11); Magenta dash-dotted: lower-bound (LB) (13); black dashed: approximation (15).

B (simulations here are more accurate than those in [5], which, however, already showed a good match), but also in case C, where the end-to-end RP1 model developed in [2] was unable to match the simulated SNR at very large powers where NLI-induced droop is significant (Cfr. [2] Fig. 5, label “Unm.”); the local-RP1 power-renormalized concatenation implicit in the GDF is instead able to well reproduce the SNR even in deep “signal depletion” by NLI. Note also that, although the GDF assumes uncorrelated noises at each span, our use of the span-averaged NLI coefficient allows us to have good fit also in links where span-by span correlations are significant, as in our 3 cases where Fig. 3 shows a marked variation of α_{NL} with span number N .

Next note that the GDF is always below the GN and its asymptotes have a different slope than those of the GN. As already noted in Fig. 2, this is an artifact of the dB representation of the SNR, since the SNR gap between the two curves is about 1/2 (in linear units) for GN-SNR above ~ 1.66 (2.2 dB).

Finally, we note that UB and LB and approximation (15) are basically coinciding with the GDF in cases A and B on the shown scale, and they become visible in the tails of the SNR “bell-curve” in case C. The gap to UB, LB and (15) is quite small, as already seen in Fig. 2. In particular, approximation (15) is the best among all, and is basically coinciding with the GDF over most of the shown ranges.

To test the resilience of the GDF at low dispersion, Fig. 5 shows, for the same parameters as case C except dispersion, the GDF-SNR versus launch power (solid), along with SSFM simulations (symbols), when dispersion is decreased from 3.8 down to 1 ps/nm/km. We see that the GDF-SNR well reproduces the simulated SNR over the whole power range down to dispersions of 1 ps/nm/km.

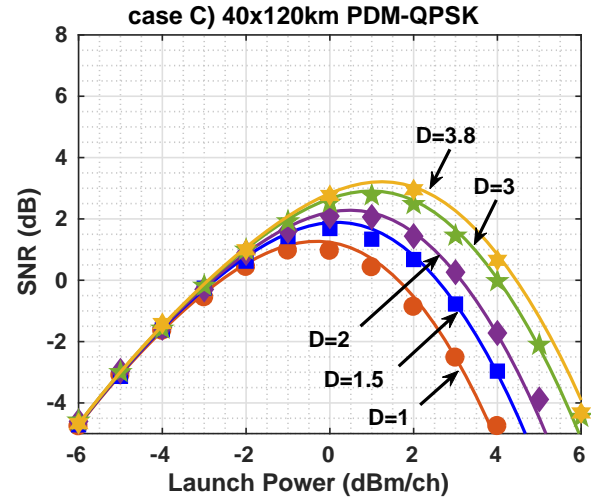


Figure 5. Case C) SNR versus launch power when lowering fiber dispersion D from 3.8 down to 1 ps/nm/km. Symbols: simulations. Solid: GDF.

A. Comparisons with the GN formula

Since the GN is the reference formula for nonlinear propagation with coherent detection, it is important to quantify its gap in performance to the GDF.

SNR gap: We here discuss the gap from SNR_{GN} eq. (17) to SNR_{GDF} eq. (18). The bounds we have found all hint at a 1-1 relation between the two SNRs. This is not exactly so, but almost. Fig. 6 plots the gap $SNR_{GN}(dB) - SNR_{GDF}(dB)$ versus $SNR_{GN}(dB)$. Symbols for the three cases (diamonds for case A, squares for case B and circles for case C) indicate the exact gap between the theoretical SNRs (we measure the gap from Fig. 4 in each case scanning from low to high power, and report the values in Fig. 6), while the dashed lines indicate the gap as expressed by the best approximation (15). Especially for case C (circles) it is evident that the SNR_{GDF} is not a 1-1 function of SNR_{GN} , but to a good extent we may

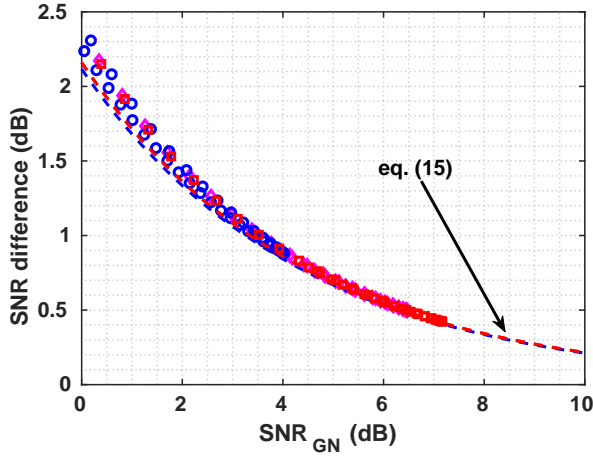


Figure 6. Gap $SNR_{GN}(dB) - SNR_{GDF}(dB)$ versus $SNR_{GN}(dB)$. Symbols (diamonds for case A, squares case B, circles for case C): exact gap, as visible in Fig. 4. Dashed: approximation (15).

well approximate the gap for all systems by eq. (15). The gap does not exceed 2.5dB for SNR_{GN} down to 0 dB.

Optimal power at max SNR: The optimal power P_o at maximum SNR is obtained in the GN model by setting the derivative of SNR_{GN} w.r.t. P to zero, yielding the condition $\beta = 2\alpha_{NL}P_o^3$ (i.e., ASE is twice the NLI at P_o) and the explicit optimal GN power $P_{oGN} = (\beta/2/\alpha_{NL})^{1/3}$.

Similarly, the GDF-SNR is maximum at the power P_o that makes the total droop $\chi(P_o)$ closest to 1, leading to the condition $\beta = \frac{2}{\chi(P_o)}\alpha_{NL}P_o^3$, i.e., ASE is *slightly more than twice* the NLI at P_o . This leads to $P_o = P_{oGN}\chi^{1/3} \lesssim P_{oGN}$, since the droop per span $\chi = \chi_a\chi_r$ is always practically very close to 1. Thus the optimal P_o for the GDF is in practice the same as in the GN case,

Spectral efficiency per mode: A lower-bound on the capacity per mode of the nonlinear optical channel for dual-polarization transmissions is obtained from the equivalent additive white Gaussian noise (AWGN) Shannon channel capacity, i.e., by considering the NLI as an additive white Gaussian process independent of the signal. Hence a lower-bound on spectral efficiency per mode is [4], [10]: $SE = 2\log_2(1 + SNR)$ [b/s/Hz]. Its top value SE_o is achieved at P_o using its corresponding top SNR.

For fixed distance, symbol rate, and noise figure, the GDF- and GN-SNR just depend on the NLI per-span parameter α_{NL} . The α_{NL} values for the AWGN capacity-achieving Gaussian modulation are reported with filled circles in Fig. 3 for both the EX2000 and the NZDSF links.

Fig. 7(a) reports (a lower-bound to) the top SE_o

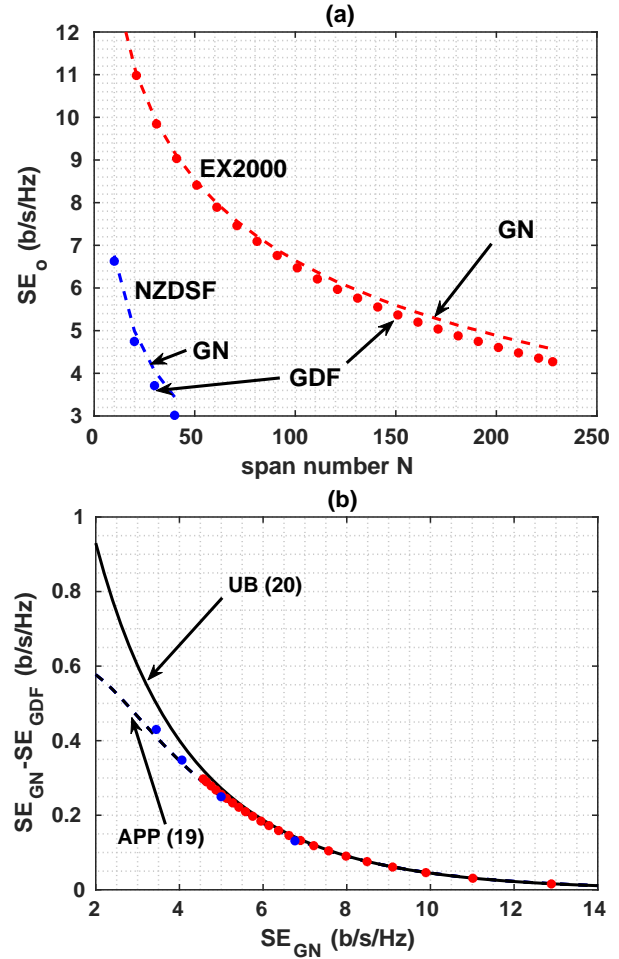


Figure 7. (a) (lower-bound to) top spectral efficiency SE_o (b/s/Hz) versus span number N , obtained for the EX2000 (case A/B) and the NZDSF (case C) links with Gaussian modulation. Dashed: GN model. Filled circles: GDF. (b) Filled circles: gap from GN to GDF SE versus GN-SE. Solid: UB (20). Dashed: approximation (19).

versus span number N for both GN (dashed) and GDF (filled circles) obtained for the EX2000 and the NZDSF links with Gaussian modulation. The figure shows that a noticeable departure of the correct GDF-SE from the GN-SE occurs only at GN-SE values below 5 b/s/Hz.

We prove in Appendix C that the SE gap from GN to GDF $\Delta SE \triangleq SE_{GN} - SE_{GDF}$ is well approximated at large N and at all powers (not only at top) by

$$\Delta SE \cong \frac{2}{\ln(2)} \frac{SNR_{GN}}{1 + 2SNR_{GN} + 2SNR_{GN}^2} \quad (19)$$

and upper bounded by

$$\Delta SE \leq \frac{1}{\ln(2)[SNR_{GN} + \frac{1}{2}]} \quad (20)$$

which are plotted in Fig. 7(b) versus SE_{GN} in dashed and solid line, respectively, together with the exact gap (filled circles). Curve (19) can be taken as a good approximation to all shown cases. From the figure, it is seen that the GN model over-estimates SE by less than 0.35 [b/s/Hz] at SE predicted by the GN model

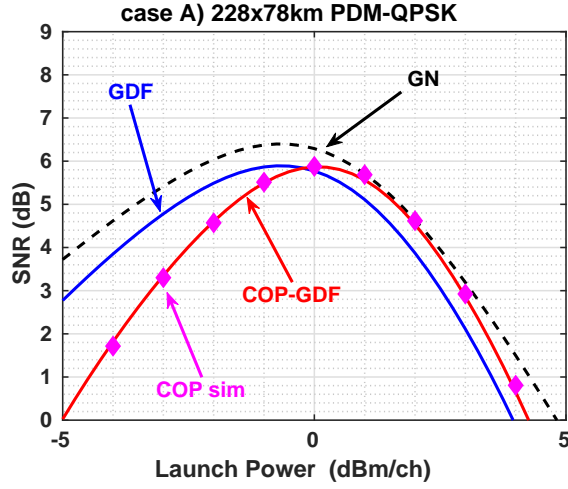


Figure 8. Case A) SNR versus launch power when amplifier bandwidth is $B_a = 60B_{rx}$, $B_{rx} = 34.17$ GHz, and ASE unfiltered. 16 PDM-QPSK channels, spacing $\Delta f = 37.5$ GHz. Symbols: simulations with COP saturation power $16P_t$. We show: the GN (17) and the raw GDF (18) (where $B \rightarrow B_{rx}$ and $P \rightarrow P_t$); and the COP-GDF, eqs. (23), (26).

above 4 [b/s/Hz], and over-estimates SE by between 0.6 and 0.9 [b/s/Hz] at $SE_{GN} = 2$ [b/s/Hz].

VI. LIMITS OF THE GDF

Unfortunately, when the amplified modes M_a and amplified bandwidth B_a exceed the signal modes M and signal occupied bandwidth $B = N_c B_{rx}$ (possible gaps between WDM channels are not counted), the GDF ceases to be accurate, and the *amplifier fill-in efficiency*:

$$\eta_A \triangleq \frac{MN_c}{M_a N_a} \quad (21)$$

with $N_a \triangleq B_a/B_{rx}$, plays a major role in setting performance.

As a numerical example, we consider the 228x78km 16-channel single-mode ($M = M_a = 1$) PDM-QPSK case study A, but now ASE is present over the whole amplified (and simulated) bandwidth $B_a = 60B_{rx}$, with $B_{rx} = 34.17$ GHz. In this system we have $\eta_A = 0.266$. This small number should be checked against the value $\eta_A = 0.91$ for case A in Fig. 4, where ASE is filtered over the WDM bandwidth and the basic GDF very well matches simulations.

Fig. 8 shows the per-tributary SNR versus launch power per tributary P_t (saturation power is in general $P = MN_c P_t$). Symbols are SSFM simulations. We also see in solid line the GN (17) and the raw GDF (18) (where in the referenced equations we set $B \rightarrow B_{rx}$ and $P \rightarrow P_t$). We note that with a low η_A the GDF ceases to well match the simulations. This is mostly due to the fact that, because of the relevant out-of-band ASE, the actual ASE-droop is larger and the actual

NLI-droop is smaller than what the GDF predicts. The next sub-section explains the tricks necessary to modify the basic GDF to cope with such a scenario.

A. The COP-GDF

Let $P_s(N)$, $P_a(N)$, $P_r(N)$ be the total cumulated signal, ASE and NLI redistribution power from the link input up to the output of span N . Assuming equal per-tributary powers, at the per-tributary receiver the SNR is:

$$\begin{aligned} SNR &= \left(\frac{P_s(N)}{MN_c} \right) / \left(\frac{P_a(N)}{M_a N_a} + \frac{P_r(N)}{MN_c} \right) \\ &= \frac{P_s(N)}{P_a(N)\eta_A + P_r(N)} \end{aligned} \quad (22)$$

where we assumed that NLI is the same at all tributaries and exists only over the same modes/spectral range as the signal multiplex. It is evident from (22) that SNR evaluation, differently from the basic GDF (7), now requires a separate evaluation of both $P_a(N)$ and $P_r(N)$. These can be calculated explicitly as shown in (36) in Appendix A, yielding

$$SNR = \frac{\prod_{m=1}^N \chi_m}{\sum_{k=1}^N [(\chi_a^{-1} - 1)\chi_{rk}^{-1}\eta_A + \chi_{rk}^{-1} - 1] \prod_{m=k}^N \chi_m} \quad (23)$$

which requires an explicit evaluation of the ASE droop χ_a (30) and of the redistribution droop χ_{rk} (32).

Specifically, regarding $\chi_a = (1 + SNR_{a1}^{-1})^{-1}$, this is span-independent, since $\delta P_i = M_a N_a h\nu F B_{rx}$, so that

$$\begin{aligned} SNR_{a1} &\triangleq \frac{P}{\delta P_i \mathcal{L}^{-1}} = \frac{MN_c P_t}{M_a N_a h\nu F B_{rx} \mathcal{L}^{-1}} \\ &= \eta_A P_t / \beta \end{aligned} \quad (24)$$

where we used definition of β (eq.(16) where $B \rightarrow B_{rx}$), and the definition of η_A (21).

Regarding the NLI droop $\chi_{rk} = (1 + SNR_{r1k}^{-1})^{-1}$ in eq. (32), this is now span-dependent because, due to the COP constraint, the out-of-band/mode ASE (O-ASE) reduces the *effective* tributary power P_e that generates NLI, more and more as the spans increase.

To find the correct per-tributary effective power $P_e(k)$ generating NLI at span k we reason as follows. At each span $k = 1, \dots, N$, the total power that effectively contributes to the NLI generation is not $P = MN_c P_t$, but P minus the O-ASE power entering span k , $P_{ASE,O}(k)$, which we now calculate.

The locally generated output O-ASE at each amplifier is $\beta' = \beta N_a (M_a - M) + \beta (N_a - N_c) M$, i.e., the sum of the whole ASE over non-signal modes and the out-of-band ASE on signal modes. With our definitions, this simplifies to $\beta' = \beta (\frac{1}{\eta_A} - 1) MN_c$. Hence the cumulated (and drooped) O-ASE up to span k is

$$P_{ASE,O}(k) \triangleq \beta' (\chi_2 \cdots \chi_{k-1} + \chi_3 \cdots \chi_{k-1} + \dots + \chi_{k-1} + 1)$$

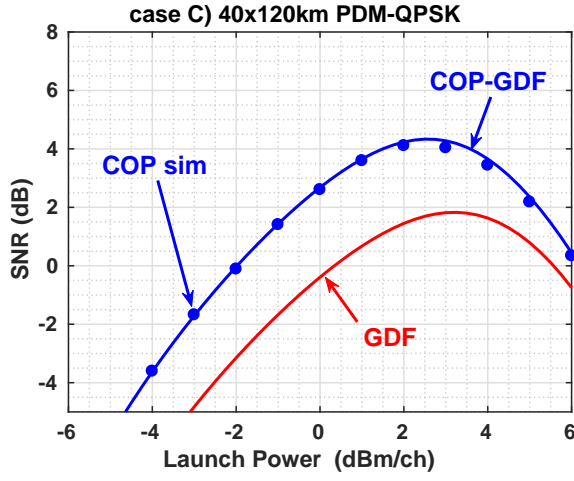


Figure 9. Case C) SNR versus launch power P_t , Cfr. Fig. 4 (15-channel 49Gb PDM-QPSK 40x120km NZDSF link with $\eta_A = 0.98$). ASE filtered on WDM bandwidth, but now channel spacing has doubled to $\Delta f = 100$ GHz, yielding an amplifier fill-in efficiency $\eta_A = 0.49$. Symbols: simulations with COP saturation power $15P_t$. We show: the basic GDF (18) where $B \rightarrow B_{rx} = 49\text{GHz}$ and $P \rightarrow P_t$, and the COP-GDF, eq. (23),(26).

where the final 1 is due to the O-ASE generated at amplifier $k-1$ which is not drooped. By approximating each droop as just the ASE droop: $\chi_j \cong \chi_a$ we thus finally get the effective power and the single-span nonlinear SNR as

$$\begin{cases} P_e(k) = \frac{P - P_{ASE,O}(k)}{MN_c} \cong P_t - \beta \left(\frac{1}{\eta_A} - 1 \right) \frac{1 - \chi_a^{k-1}}{1 - \chi_a} \\ SNR_{rk} = \frac{P}{\delta P_{rk}} \equiv \frac{P_t}{\alpha_{NL} P_e(k)^3} \end{cases} \quad (25)$$

In summary, the resulting improved SNR formula, which we call the *COP-GDF*, is calculated by eq. (23), where using (24) and (25) we have

$$\begin{cases} \chi_a^{-1} = 1 + \beta / (\eta_A P_t) \\ \chi_{rk}^{-1} \cong 1 + \alpha_{NL} P_t^2 \left(1 - \frac{\beta}{P_t} \left(\frac{1}{\eta_A} - 1 \right) \frac{1 - \chi_a^{k-1}}{1 - \chi_a} \right)^3 \end{cases} \quad (26)$$

For case study A, Fig. 8 also reports the COP-GDF and shows that it well matches simulations. Similar results are obtained for case B and are not reported.

We show in Fig. 9 for case study C what happens when channel spacing is doubled to 100 GHz with respect to Fig. 4, and thus the amplifier fill-in efficiency is halved to $\eta_A = 0.49$. We see that the basic GDF formula badly fails, but the COP-GDF well matches the SSFM simulations.

VII. THE CONSTANT-GAIN CASE

For CG amplifiers, the extension of the GN model to include the nonlinear signal-noise interaction, and its induced signal power depletion, was tackled in [19] with a rigorous end-to-end RP1 model (which inspired

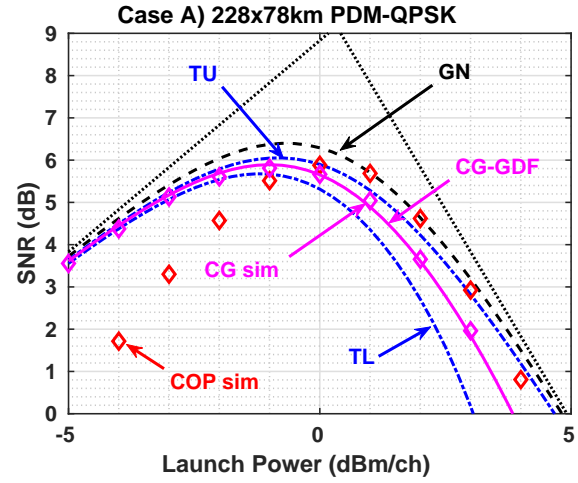


Figure 10. Case A) SNR versus launch power P_t when amplifier bandwidth is $B_a = 60\Delta f$, $\Delta f = 37.5$ GHz, and ASE unfiltered, as in Fig. 8. Symbols: simulations for both CG and COP. We show: the GN formula (dash); TU and TL formulas, eq. (27),(28) (dash-dot); and the CG-GDF, eq. (23),(29).

the COP-amplifier end-to-end RP1 model in [2]), and heuristically in [18]. While the RP1 model in [19] has the same intrinsic inability as the model in [2] to cope with the NLI-induced droop at large power, the heuristic models in [18] do go beyond the RP1 limits. We next review such models, and introduce our new contribution, namely the CG-GDF, that uses the Turin's group physical intuitions [18] to extend the COP-GDF ideas and yield a very accurate SNR estimation formula even for the CG case.

The CG-SNR formulas in [18] are the following:

1) *TU*: it calculates the formula $SNR = \frac{P_t}{N\beta + P_{NLI}}$ with

$$P_{NLI} = \alpha_{NL} \sum_{n=0}^{N-1} (P_t + n\beta)^3 \quad (27)$$

that approximately accounts for ASE-signal nonlinear interaction by suitably modifying the estimated NLI variance [18, eq. (5)]³. Note that this formula assumes that the ASE useful for nonlinear calculations is the one over the signal bandwidth, since O-ASE is ineffective for CG amplifiers.

2) *TL*: it calculates the formula

$$SNR = \frac{P_t - P_{NLI}}{N\beta + P_{NLI}} \quad (28)$$

with P_{NLI} as in (27).

For case study A), Fig. 10 reports the tributary SNR versus launch power P_t for both CG and COP amplifiers, when amplifier bandwidth is $B_a = 60B_{rx}$ and ASE is unfiltered, same as in Fig. 8. Symbols are the simulations for both CG and COP amplifiers, the

³Summation in [18] runs 1 to N , but in our simulations the launched power is without ASE, hence we sum 0 to $N - 1$.

dashed curve is the GN formula, the dash-dotted curves are the TU and TL formulas, and the solid curve is the new CG-GDF formula that we will describe below.

Regarding SSFM simulations, we first note a shift of the CG SNR with respect to the COP SNR, much in line with the results in [5, Fig 2(b)]. The low-power SNR of the CG case is larger than the COP case because it does not experience ASE-induced droop; the high-power SNR of the CG case is smaller than the COP case because of the span-by-span increase of power in CG that generates nonlinearity.

Regarding the T-formulas, we note that TU overestimates the simulated CG SNR, while TL with depletion under-estimates the CG SNR. All the CG curves (simulations, T-formulas, CG-GDF) at low powers tend to coincide with the theoretical GN curve, as they should.

A. The CG-GDF and the improved TU

The trouble with the T-formulas is that they try to model a strongly nonlinear system with an amended end-to-end RP1 system. The amendments, however, do contain the correct physical intuition. So the key to the new CG-GDF is to use the intuition [18] about the effective power for NLI generation, eq. (27), but with a re-normalized RP1 per-span model instead of the end-to-end RP1 GN model.

In CG mode we can consider only the ASE and NLI on the per-tributary bandwidth (O-ASE does not affect the SNR). The power-flow diagram is again given by Fig. 1(d), where now we have $\chi_a = 1$, i.e., no ASE droop, and $\delta P_i \mathcal{L}^{-1} \equiv \beta$. As in (27), we now let $\delta P_{rk} = \alpha_{NL}(P_t + (k-1)\beta)^3$.

The new SNR formula, which we call the *CG-GDF*, is thus calculated by eq. (23), where we now use $\chi_k = \chi_{rk}$, $\eta_A = 1$, and replace

$$\begin{cases} (\chi_a^{-1} - 1) \rightarrow \beta/P_t \\ \chi_{rk}^{-1} \rightarrow 1 + \alpha_{NL}P_t^2(1 + (k-1)\frac{\beta}{P_t})^3. \end{cases} \quad (29)$$

In the example of case A), Fig. 10 shows an excellent match between CG-simulations and the CG-GDF. A similarly good match is obtained in the remaining cases B and C.

VIII. CONCLUSIONS

In this paper, we presented an analytical model to fully theoretically support the GDF disclosed by Antona *et al.* in [5], [6], which includes various fiber power-redistribution mechanisms such as Kerr nonlinearity, GAWBS, and internal and external crosstalk. We verified the GDF against simulations in three published case studies drawn from [2], [5].

We provided upper and lower bounds to the GDF. Using the tightest upper-bound we provided analytical

expressions of the SNR and Shannon spectral efficiency (SE) gaps from the GN formula to the GDF. We showed that the gaps can be effectively expressed only in terms of the GN-predicted SNR and SE. We showed that the SE gap (per mode) is bounded between 0.6 and 0.9 b/s/Hz when the GN-SE is as low as 2 b/s/Hz, and it decreases as the GN-SE increases, e.g., it is less than 0.2 b/s/Hz when the GN-SE is above 6 b/s/Hz.

We extended the GDF to the case where ASE has larger bandwidth/mode occupancy than the signal. The resulting COP-GDF equation depends only on the amplifier fill-in efficiency η_A , eq. (21), and was found to very well match simulations in all considered cases. Finally, we extended the theory to include constant-gain amplifier chains, and we derived the new CG-GDF SNR expression that matches simulations better than any other previously known formula.

One of the key theoretical results is that the end-to-end model underlying all GDF expressions is a concatenation of per-span RP1 models with end-span power renormalization. This fact allows the GDFs to well reproduce the SNR of highly nonlinear systems, well beyond the RP1 limit of the GN model. The model is reminiscent of multi-stage backpropagation, that combines the benefits of split-step and perturbation-based approaches.

APPENDIX A: GDF FOR INHOMOGENEOUS SPANS

The generalization of the GDF model to the inhomogeneous case goes as follows. The k -th span now has input power P_{k-1} , fiber span loss $\mathcal{L}_k < 1$ and an end-span amplifier operated in COP mode with fixed output power P_k , $k = 0, \dots, N$ (where P_0 is the launched power) and a gain G_k which, in absence of ASE-induced droop, would be $G_k = P_k/(P_{k-1}\mathcal{L}_k)$. With ASE droop the gain is smaller by a factor $\chi_{ak} < 1$. The power flow diagram for the inhomogeneous case is similar to the homogenous case of Fig. 1, where i) all quantities are span- k dependent; ii) the multiplicative output factor in diagrams (c), (d) is now $\chi_{ak}P_k/P_{k-1}$ instead of only χ_a ; iii) in diagram (d) the input sub-block has input/output power P_{k-1} , while the output sub-block has P_{k-1} in and P_k out.

From the modified diagram (d) we thus derive:

1) the power balance at the output sub-block: $(P_{k-1} + \delta P_{ik}\mathcal{L}_k^{-1})\chi_{ak}\frac{P_k}{P_{k-1}} = P_k$, which yields

$$\chi_{ak} = (1 + \frac{\delta P_{ik}\mathcal{L}_k^{-1}}{P_{k-1}})^{-1} \triangleq (1 + SNR_{a1k}^{-1})^{-1} \quad (30)$$

where we implicitly defined the SNR degraded by ASE at the single amplifier as

$$SNR_{a1k} \triangleq \frac{P_{k-1}}{\delta P_{ik}\mathcal{L}_k^{-1}}. \quad (31)$$

2) the power balance at the input sub-block: $(P_{k-1} + \delta P_{rk})\chi_{rk} = P_{k-1}$, which yields

$$\chi_{rk} = (1 + \frac{\delta P_{rk}}{P_{k-1}})^{-1} \triangleq (1 + \text{SNR}_{r1k}^{-1})^{-1} \quad (32)$$

where we implicitly defined the SNR degraded by power redistribution at the single amplifier as

$$\text{SNR}_{r1k} \triangleq \frac{P_{k-1}}{\delta P_{rk}}. \quad (33)$$

Define the span total droop as the product of addition and redistribution droops: $\chi_k \triangleq \chi_{rk}\chi_{ak}$. The power block diagram of the k -th span in (modified) diagram (d) shows that the total span power-gain seen by the transiting signal is $(P_k/P_{k-1})\chi_k$, hence the desired multiplex signal power at the output of the N -th amplifier is

$$P_s(N) = P_0 \prod_{k=1}^N (P_k/P_{k-1})\chi_k = P_N \prod_{k=1}^N \chi_k$$

so that the total noise power after N spans is $P_a(N) + P_r(N) = P_N(1 - \prod_{k=1}^N \chi_k)$.

Hence the OSNR at the output of the chain from amplifiers 1 to N , i.e., the ratio of total multiplex signal power to total noise power at the output of the N -th amplifier, is obtained as

$$\text{OSNR} = \frac{1}{\left[\prod_{k=1}^N (1 + \frac{1}{\text{SNR}_{a1k}})(1 + \frac{1}{\text{SNR}_{r1k}}) \right] - 1} \quad (34)$$

which leads to the general product rule for inverse droops, eq. (9) in the main text.

For the calculation of the per-tributary SNR it is necessary instead to have the individual expression of $P_a(N)$, $P_r(N)$, as seen in eq. (22) in the main text. It is possible to read off the modified diagram (d) the update rule for useful signal, additive and redistribution noise at any span k as:

$$\begin{aligned} P_s(k) &= P_s(k-1)\chi_k(P_k/P_{k-1}) \\ P_a(k) &= (P_a(k-1) + \delta P_{ik}\mathcal{L}_k^{-1}\chi_{rk}^{-1})\chi_k(P_k/P_{k-1}) \\ P_r(k) &= (P_r(k-1) + \delta P_{rk})\chi_k(P_k/P_{k-1}) \end{aligned} \quad (35)$$

with initial conditions: $P_s(0) = P_0$, $P_a(0) = P_r(0) = 0$. The second and third recursions are of the kind: $u(k) = (u(k-1) + b_k)a_k$, whose general solution when $u(0) = 0$ is: $u(N) = \sum_{k=1}^N b_k \prod_{m=k}^N a_m$.

Hence, using $\delta P_{ik}\mathcal{L}_k^{-1} \equiv P_{k-1}(\chi_{ak}^{-1} - 1)$ and $\delta P_{rk} \equiv P_{k-1}(\chi_{rk}^{-1} - 1)$ from (30),(32), the formal solutions are

$$\begin{aligned} P_s(N) &= P_N \prod_{m=1}^N \chi_m \\ P_a(N) &= P_N \sum_{k=1}^N (\chi_{ak}^{-1} - 1)\chi_{rk}^{-1} \prod_{m=k}^N \chi_m \\ P_r(N) &= P_N \sum_{k=1}^N (\chi_{rk}^{-1} - 1) \prod_{m=k}^N \chi_m \end{aligned} \quad (36)$$

Although this closed-form solution is pleasing, the recursion (35) is the one we use for calculations.

APPENDIX B: CAVEATS IN α_{NL} ESTIMATION FROM SSFM SIMULATIONS

This appendix discusses some caveats in estimating from SSFM simulations the span-average nonlinear coefficient α_{NL} to be used in the theoretical formulas, whenever the end-to-end system is highly nonlinear, way beyond the RP1 limits. Let the generic tributary complex received field be $A_{rx}(t)$. In absence of ASE we know from the GDF model that we have only redistribution droop: $\chi \equiv \chi_r = (1 + \alpha_{NL}P^2)^{-1}$, and the received power is

$$\begin{aligned} \langle |A_{rx}(t)|^2 \rangle &= P = \chi^N P + (1 - \chi^N)P \\ &\equiv \chi^N P(1 + V_{NLI}) \end{aligned}$$

where the brackets denote time averaging, and we implicitly defined the variance of the normalized end-to-end NLI

$$V_{NLI}(P) \triangleq \chi^{-N} - 1 = (1 + \alpha_{NL}P^2)^N - 1. \quad (37)$$

Now define⁴

$$\alpha_{NL}(P) \triangleq \frac{V_{NLI}(P)}{NP^2} = \frac{(1 + \alpha_{NL}P^2)^N - 1}{NP^2} \quad (38)$$

as the *span-averaged power-dependent NLI coefficient*. At small powers it coincides with the NLI coefficient α_{NL} of the *per-span* RP1 expansion, since $\lim_{P \rightarrow 0} V_{NLI}(P)/(NP^2) = \alpha_{NL}$. In a truly end-to-end RP1 system, the quantity $\alpha_{NL}(P)$ should at all powers coincide with α_{NL} . At powers for which $\alpha_{NL}(P)$ markedly departs from α_{NL} , the end-to-end line ceases to be RP1.

An estimation $\hat{V}_{NLI}(P)$ of the value of $V_{NLI}(P)$ in (38) is routinely obtained from the samples of the received constellation scatter diagram.

We ran SSFM simulations of the PDM-QPSK system in [5], case A. Fig. 11 shows a plot of the

⁴Please note the use of boldface, to distinguish $\alpha_{NL}(P)$ which is P dependent, from the span-average coefficient α_{NL} which is power independent.

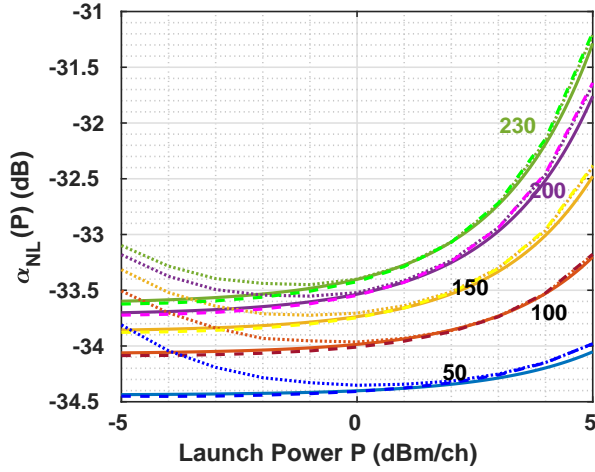


Figure 11. dB-value of span-averaged power-dependent NLI coefficient $\alpha_{NL}(P)$ [mW^{-2}] in eq. (38) versus launch power P (thick solid) and its estimate $\hat{\alpha}_{NL}(P) \triangleq \hat{V}_{NLI}(P)/(NP^2)$ from simulated scatter diagrams in absence of ASE (dotted for a step-size with nonlinear phase $10^{-3}(\text{rad})$, dashed for $5 \cdot 10^{-4}(\text{rad})$). Values used in theoretical formula: $\alpha_{NL} = [-34.44, -34.07, -33.87, -33.72, -33.62]$ (dB) for $N = [50, 100, 150, 200, 230]$ spans.

estimated span-averaged power-dependent NLI coefficient $\hat{\alpha}_{NL}(P) \triangleq \hat{V}_{NLI}(P)/(NP^2)$ [mW^{-2}] (dotted for a standard step-size with nonlinear phase per span (NLP) $10^{-3}(\text{rad})$, dashed for $5 \cdot 10^{-4}(\text{rad})$) and the theoretical expression (38) in thick solid line, in which the best-fitting values $\alpha_{NL} = [-34.44, -34.07, -33.87, -33.72, -33.62]$ (dB) for 5 values of the span number $N = [50, 100, 150, 200, 230]$ were used to match the low-power values of $\alpha_{NL}(P)$ to simulations with the most precise NLP. Such best-fitting α_{NL} values are those used in the theoretical formulas in the text, and are reported in Fig. 3 along with those of cases B) and C).

Fig. 11 highlights two interesting facts:

1) for the system in case A, with a standard choice of the step size the estimated variance does not flatten out at low powers, as it should when the end-to-end line behaves as a truly RP1 system. So care should be taken to verify that the simulation-based estimation of α_{NL} is done with the correct step size;

2) when the end-to-end system is more nonlinear than an RP1 system, the new analytical expression (38) for $\alpha_{NL}(P)$ well matches the simulated quantity $\hat{\alpha}_{NL}(P) \triangleq \hat{V}_{NLI}(P)/(NP^2)$, a further indication that the locally-RP1, power-renormalized concatenation underlying the GDF well models such a highly nonlinear system.

In practice, normally only a single low-power end-to-end simulation (with a correct step-size) can be run to estimate the value of the span-averaged α_{NL} to be used in the theory as $(\hat{V}_{NLI}(P)+1)^{1/N}-1/P^2$, as per (37). Alternatively, one may use the EGN model [25]–

[28] to get the end-to-end NLI coefficient and then divide the result by N to get the span-average α_{NL} .

APPENDIX C: SE GAP APPROXIMATIONS

This appendix derives two approximations of the SE decrease due to droop with respect to the GN value, as shown in Sec. V-A.

The SE decrease (at any power P , not only at top value P_0) is:

$$\Delta SE \equiv SE_{GN} - SE_{GDF} = 2 \log_2 \left(\frac{1 + SNR_{GN}}{1 + SNR_{GDF}} \right)$$

Thus using the UB (11) and at large N we get:

$$\begin{aligned} \Delta SE &\geq 2 \log_2 \left(\frac{1 + SNR_{GN}}{1 + \frac{2(SNR_{GN})^2}{1+2SNR_{GN}}} \right) \\ &= 2 \log_2 \left(\frac{1 + 3SNR_{GN} + 2(SNR_{GN})^2}{1 + 2SNR_{GN} + 2(SNR_{GN})^2} \right) \\ &= \frac{2}{\ln(2)} \ln \left(1 + \frac{SNR_{GN}}{1 + 2SNR_{GN} + 2(SNR_{GN})^2} \right) \\ &\leq \frac{2}{\ln(2)} \frac{SNR_{GN}}{1 + 2SNR_{GN} + 2(SNR_{GN})^2} \end{aligned}$$

which is approximation (19) in the main text. It is neither an upper nor a lower bound.

Using instead the LB (13) at large N we get

$$\begin{aligned} \Delta SE &\leq 2 \log_2 \left(\frac{1 + SNR_{GN}}{1 + SNR_{GN} - \frac{1}{2}} \right) \\ &= 2 \log_2 \left(1 + \frac{1/2}{SNR_{GN} + \frac{1}{2}} \right) \\ &\leq \frac{1}{\ln(2) [SNR_{GN} + \frac{1}{2}]} \end{aligned}$$

which is the UB (20).

REFERENCES

- [1] C. R. Giles and E. Desurvire, "Propagation of Signal and Noise in Concatenated Erbium-Doped Fiber Optical Amplifiers", *J. Lightw. Technol.*, vol. 9, no. 2, pp. 147-154, Feb. 1991.
- [2] A. Ghazisaeidi, "A Theory of Nonlinear Interactions between Signal and Amplified Spontaneous Emission Noise in Coherent Wavelength Division Multiplexed Systems," *J. Lightw. Technol.*, vol. 35, pp. 5150–5175, Dec. 2017.
- [3] O. V. Sinkin *et al.*, "Maximum Optical Power Efficiency in SDM-Based Optical Communication Systems," *Photon. Technol. Lett.*, vol. 29, no. 13, pp. 1075-1077, Jul. 2018.
- [4] O. V. Sinkin *et al.*, "SDM for Power-Efficient Undersea Transmission," *J. Lightw. Technol.*, vol. 36, no. 2, pp. 361-371, Jan. 2018.
- [5] J.-C. Antona, A. Carbo Méséguer, and V. Letellier, "Transmission Systems with Constant Output Power Amplifiers at Low SNR Values: a Generalized Droop Model," in *Proc. Opt. Fiber Commun. (OFC)*, San Diego (CA), 2019, paper M1J.6.
- [6] J.-C. Antona *et al.*, "Performance of open cable: from modeling to wide scale experimental assessment," in *Proc. SubOptic*, New Orleans (LA), 2019.

- [7] G. Bosco *et al.*, "Performance prediction for WDM PM-QPSK transmission over uncompensated links," in Proc. *Opt. Fiber Commun. (OFC)*, San Diego (CA), 2011, paper OThO7.
- [8] E. Grellier and A. Bononi, "Quality parameter for coherent transmissions with Gaussian-distributed nonlinear noise," *Opt. Exp.*, vol. 19, no. 13, pp. 12781--12788, Jun. 2011.
- [9] A. Carena, *et al.*, "Modeling of the Impact of Non-Linear Propagation Effects in Uncompensated Optical Coherent Transmission Links," *J. Lightw. Technol.*, vol. 30, no. 10, pp. 1524-1539, may 2012.
- [10] P. Poggiolini, "The GN model of non-linear propagation in uncompensated coherent optical systems," *J. Lightw. Technol.*, vol. 30, no. 24, pp. 3857--3879, Dec. 2012.
- [11] A. Bononi, J.-C. Antona, A. Carbo Méséguer, P. Serena, "A model for the generalized droop formula," in Proc. *European Conf. on Optical Commun. (ECOC)*, Dublin, Ireland, 2019, paper W.1.D.5. Also available at arXiv:1906.08645.
- [12] A. Vannucci, P. Serena, and A. Bononi, "The RP method: a new tool for the iterative solution of the nonlinear Schroedinger equation," *J. Lightw. Technol.*, vol. 20, pp. 1102--1112, Jul. 2002.
- [13] P. Poggiolini, G. Bosco, A. Carena, V. Curri, F. Forghieri, "A Detailed Analytical Derivation of the GN Model of Non-Linear Interference in Coherent Optical Transmission Systems," Available: arXiv:1209.0394, [physics.optics] (2012).
- [14] P. Johannisson and M. Karlsson, "Perturbation analysis of nonlinear propagation in a strongly dispersive optical communication system," *J. Lightw. Technol.* vol. 31, pp. 1273-1282 (2013).
- [15] A. Bononi and P. Serena, "An alternative derivation of Johannisson's regular perturbation model," Available: arXiv:1207.4729, [physics.optics] (2012).
- [16] M. Secondini, D. Marsella, and E. Forestieri, "Enhanced split-step Fourier method for digital backpropagation," in Proc. *European Conf. on Optical Commun. (ECOC)*, Cannes, France, 2014, paper We.3.3.5.
- [17] X. Liang and S. Kumar, "Multistage perturbation theory for compensating intra-channel impairments in fiber optic systems," *Opt. Exp.*, vol. 22, no. 24, pp. 29733-29745, Dec. 2014.
- [18] P. Poggiolini, A. Carena, Y. Jiang, G. Bosco, V. Curri, and F. Forghieri, "Impact of low-OSNR operation on the performance of advanced coherent optical transmission systems," in Proc. *European Conf. on Optical Commun. (ECOC)*, Cannes, France, 2014, paper Mo.4.3.2.
- [19] P. Serena, "Nonlinear Signal-Noise Interaction in Optical Links With Nonlinear Equalization," *J. Lightw. Technol.*, vol. 34, no. 6, pp. 1476--1483, Mar. 2016.
- [20] G. Bosco, V. Curri, A. Carena, P. Poggolini, and F. Forghieri, "On the Performance of Nyquist-WDM Terabit Superchannels Based on PM-BPSK, PM-QPSK, PM-8QAM or PM-16QAM Subcarriers," *J. Lightw. Technol.*, vol. 29, n. 1, pp. 53-61 (2011).
- [21] H. A. Haus, "The Noise Figure of Optical Amplifiers," *Photon. Technol. Lett.*, vol. 10, no. 11, pp. 1602-1604, Nov. 1998.
- [22] F. Vacondio *et al.*, "On nonlinear distortions of highly dispersive optical coherent systems," *Opt. Exp.*, vol. 20, no. 2, pp. 1022--1032, Jan. 2012.
- [23] M. A. Bolshtyansky *et al.*, "Impact of Spontaneous Guided Acoustic-Wave Brillouin Scattering on Long-haul Transmission," in Proc. *Opt. Fiber Commun. (OFC)*, San Diego (CA), 2018, paper M4B.3.
- [24] J. M. Gené and P. J. Winzer "A Universal Specification for Multicore Fiber Crosstalk," *Photon. Technol. Lett.*, vol 31, n. 9, pp. 673-676 (2019).
- [25] A. Carena *et al.* "EGN model of non-linear fiber propagation," *Opt. Exp.*, vol. 22, no. 13, pp. 16335--16362, Jun. 2014.
- [26] P. Poggiolini *et al.*, "A Simple and Effective Closed-Form GN Model Correction Formula Accounting for Signal Non-Gaussian Distribution," *J. Lightw. Technol.*, vol. 33, no. 2, pp. 459--473, Jan. 2015.
- [27] R. Dar, M. Feder, A. Mecozzi, and M. Shtaif, "Accumulation of nonlinear interference noise in fiber-optic systems," *Opt. Exp.*, vol. 22, no. 12, pp. 14199--14211, Jun. 2014.
- [28] P. Serena, and A. Bononi, "A Time-Domain Extended Gaussian Noise Model," *J. Lightw. Technol.*, vol. 33, no. 7, pp. 1459--1472, Apr. 2015.